Verification of joint input-state estimation by means of a full scale experiment on a footbridge

Maes, K; de Roeck, G; Lombaert, G; van Nimmen, K; Lourens, Eliz-Mari; Rezayat, A; Guillaume, P

DOI
10.1201/9781315375175-43

Publication date
2016

Document Version
Accepted author manuscript

Published in
Life-Cycle of Engineering Systems: Emphasis on Sustainable Civil Infrastructure

IALCCE 2016: Fifth International Symposium on Life-Cycle Civil Engineering
October 16-19, 2016 / The Netherlands, Delft

Verification of joint input-state estimation by means of a full scale experiment on a footbridge

K. Maes & G. De Roeck & G. Lombaert
KU Leuven, Department of Civil Engineering, Leuven, Belgium

K. Van Nimmen
KU Leuven, Department of Civil Engineering, Leuven, Belgium
KU Leuven @ KAHO Sint-Lieven, Department of Civil Engineering, Ghent, Belgium

E. Lourens
Delft University of Technology, Faculty of Civil Engineering and Geosciences, Delft, The Netherlands

A. Rezayat & P. Guillaume
Vrije Universiteit Brussel, Department of Mechanical Engineering, Brussels, Belgium

ABSTRACT: This paper presents a verification of a state-of-the-art joint input-state estimation algorithm using data obtained from in situ experiments on a footbridge. A dynamic model of the footbridge is based on a detailed finite element model that is calibrated using a set of experimental modal characteristics. The joint input-state estimation algorithm is used for the identification of two impact, harmonic, and swept sine forces applied to the bridge deck. In addition to these forces, unknown stochastic forces, such as wind loads, are acting on the structure. These forces, as well as measurement errors, give rise to uncertainty in the estimated forces and system states. Quantification of the uncertainty requires determination of the power spectral density of the unknown stochastic excitation, which is identified from the structural response under ambient loading. The verification involves comparing the estimated forces with the actual, measured forces. Although a good overall agreement is obtained between the estimated and measured forces, modeling errors prohibit a proper distinction between multiple forces applied to the structure for the case of harmonic and swept sine excitation.

1 INTRODUCTION

Knowledge of the dynamic loads acting on a structure and its dynamic response is important for many engineering applications. The dynamic loads are crucial in the design process. Monitoring of these allows comparing the design loads to the actual solicitation of the structure. The response of the structure, which for example consists of strains or accelerations, can be used to check if serviceability limit states are exceeded, or to monitor the condition of the structure. In many cases, the forces applied to the structure cannot be directly measured. In addition, the response cannot be measured at all physical locations, due to practical and economical considerations. If the forces and/or the response cannot be directly obtained from measurements, system inversion techniques can be used for estimating the unmeasured quantities, hereby using a limited set of response measurements and a dynamic model of the structure.

Many force identification algorithms have been proposed in the literature (Liu and Shepard 2005, Parloo et al. 2003, Klinkov and Fritzen 2007, Nordström and Nordberg 2002, Bernal and Ussia 2015). Additionally, several state estimation algorithms have been proposed for linear as well as non-linear systems (Hernandez and Bernal 2008, Hernandez 2011). A common approach in state estimation consists of modeling the system input as zero mean Gaussian white noise and applying a Bayesian framework for state estimation (Ching and Beck 2007, Papadimitriou et al. 2011). In order to overcome the assumption of white noise system input, which is often violated in practical applications, filtering methods in the presence of unknown inputs have been developed. The algorithms are often referred to as joint input-state estimation algorithms and combine both input and state estimation, e.g. (Klinkov and Fritzen 2006, Hsieh 2010, Lourens et al. 2012, Eftekhar Azam et al. 2015).

Gillijns and De Moor (2007) have proposed an algorithm where the input estimation is performed prior to the state estimation step. This algorithm was introduced in structural dynamics by Lourens et al. (2012) and further extended in (Maes et al. 2016), for cases where accelerations are measured in the presence of unknown stochastic excitation. The algorithm can be used for force identification (Maes et al. 2016) and the estimation of the structural response at unmeasured locations, a.k.a. virtual sensing (Lourens et al. 2012).

Verification of the force identification techniques proposed in the literature is, to date, mostly based on numerical simulations, where (idealized) measurement errors are incorporated by adding white noise to the simulated response signals, or to laboratory experiments. This paper presents a full-scale verification of the joint input-state estimation algorithm proposed in (Maes et al. 2016) using data obtained from an in situ experiment on a footbridge. The algorithm is used to identify the impact, harmonic, and swept sine excitations applied to the bridge deck. The verification is performed by comparison of the estimated forces to the actual, measured forces.

The outline of the paper is as follows. Section 2 gives the extension of the joint input-state estimation algorithm. Section 3 discusses the setup of the experiments on the footbridge. Section 4 shows the derivation of a state-space model representing the dynamic behavior of the structure, starting from a detailed finite element model. Section 5 presents the selection of data for force identification. Section 6 discusses the results of the force identification. Finally, section 7 presents conclusions.

2 MATHEMATICAL FORMULATION

This section gives a brief summary of the joint input-state estimation algorithm introduced in (Maes et al. 2016).

Consider the following discrete-time combined deterministic-stochastic state-space description of a system:

$$\mathbf{x}_{[k+1]} = \mathbf{A}\mathbf{x}_{[k]} + \mathbf{B}\mathbf{p}_{[k]} + \mathbf{w}_{[k]} \tag{1}$$

$$\mathbf{d}_{[k]} = \mathbf{G}\mathbf{x}_{[k]} + \mathbf{J}\mathbf{p}_{[k]} + \mathbf{v}_{[k]} \tag{2}$$

where $\mathbf{x}_{[k]} \in \mathbb{R}^{n_\mathrm{s}}$ is the state vector, $\mathbf{d}_{[k]} \in \mathbb{R}^{n_\mathrm{d}}$ is the output vector, assumed to be measured, and $\mathbf{p}_{[k]} \in \mathbb{R}^{n_\mathrm{p}}$ is the unknown input vector, with n_s the number of system states, n_d the number of outputs, and n_p the number of inputs. The system matrices **A**, **B**, **G**, and **J** are assumed known. Throughout the derivation of the algorithm, it is assumed that the sensor network meets the conditions for instantaneous system inversion derived in (Maes et al. 2015).

The process noise vector $\mathbf{w}_{[k]} \in \mathbb{R}^{n_\mathrm{s}}$ and measurement noise vector $\mathbf{v}_{[k]} \in \mathbb{R}^{n_\mathrm{d}}$ both account for unknown excitation sources and modeling errors. The measurement noise vector $\mathbf{v}_{[k]}$ also accounts for measurement errors. The noise processes $\mathbf{w}_{[k]}$ and $\mathbf{v}_{[k]}$ are assumed to be zero mean and white, with known covariance matrices **Q**, **R**, and **S**, defined by:

$$\mathbb{E}\left\{ \begin{pmatrix} \mathbf{w}_{[k]} \\ \mathbf{v}_{[k]} \end{pmatrix} \begin{pmatrix} \mathbf{w}_{[l]}^\mathrm{T} & \mathbf{v}_{[l]}^\mathrm{T} \end{pmatrix} \right\} = \begin{bmatrix} \mathbf{Q} & \mathbf{S} \\ \mathbf{S}^\mathrm{T} & \mathbf{R} \end{bmatrix} \delta_{[k-l]} \tag{3}$$

with $\mathbf{R} > 0$, $\begin{bmatrix} \mathbf{Q} & \mathbf{S} \\ \mathbf{S}^\mathrm{T} & \mathbf{R} \end{bmatrix} \geq 0$, and $\delta_{[k]} = 1$ for $k = 0$ and 0 otherwise. $\mathbb{E}\{\cdot\}$ is the expectation operator.
Finally, it is assumed that an unbiased estimate $\hat{\mathbf{x}}_{[0|-1]}$ of the initial state is available, with error covariance matrix $\mathbf{P}_{\mathrm{x}[0|-1]}$ (i.e. $\mathbb{E}\left\{\mathbf{x}_{[0]} - \hat{\mathbf{x}}_{[0|-1]}\right\} = 0$, $\mathbf{P}_{\mathrm{x}[0|-1]} = \mathbb{E}\left\{(\mathbf{x}_{[0]} - \hat{\mathbf{x}}_{[0|-1]})(\mathbf{x}_{[0]} - \hat{\mathbf{x}}_{[0|-1]})^\mathrm{T}\right\}$). The estimate $\hat{\mathbf{x}}_{[0|-1]}$ is assumed independent on the noise processes $\mathbf{w}_{[k]}$ and $\mathbf{v}_{[k]}$ for all k.

The joint input-state estimation algorithm consists of a three-step recursive filter:

$$\hat{\mathbf{p}}_{[k|k]} = \mathbf{M}_{[k]} \left(\mathbf{d}_{[k]} - \mathbf{G}\hat{\mathbf{x}}_{[k|k-1]}\right) \tag{4}$$

$$\hat{\mathbf{x}}_{[k|k]} = \hat{\mathbf{x}}_{[k|k-1]} + \mathbf{K}_{[k]} \left(\mathbf{d}_{[k]} - \mathbf{G}\hat{\mathbf{x}}_{[k|k-1]} - \mathbf{J}\hat{\mathbf{p}}_{[k|k]}\right) \tag{5}$$

$$\hat{\mathbf{x}}_{[k+1|k]} = \mathbf{A}\hat{\mathbf{x}}_{[k|k]} + \mathbf{B}\hat{\mathbf{p}}_{[k|k]} \tag{6}$$

The first step in equation (4), referred to as the "input estimation step", yields a filtered estimate of the unknown input vector $\mathbf{p}_{[k]}$, given the measured output $\mathbf{d}_{[k]}$ up to time step k. The second step in equation (5), referred to as the "measurement update", yields a filtered estimate of the state vector $\mathbf{x}_{[k]}$. The third step in equation (6), referred to as the "time update", yields a one step ahead prediction of the state vector $\mathbf{x}_{[k+1]}$. The gain matrices $\mathbf{M}_{[k]} \in \mathbb{R}^{n_\mathrm{p} \times n_\mathrm{d}}$ and $\mathbf{K}_{[k]} \in \mathbb{R}^{n_\mathrm{s} \times n_\mathrm{d}}$ are determined such that both the input estimates $\hat{\mathbf{p}}_{[k|k]}$ and the state estimates $\hat{\mathbf{x}}_{[k|k]}$ are minimum variance and unbiased (MVU) (Gillijns & De Moor 2007), i.e. the uncertainty on the force and state estimates is minimized, and the error on the estimated forces $\hat{\mathbf{p}}_{[k|k]}$ and states $\hat{\mathbf{x}}_{[k|k]}$ does not depend on the actual forces $\mathbf{p}_{[k]}$. The gain matrices depend on the noise covariance matrices **Q**, **R**, and **S**, on the forces to be estimated, as well as on the sensor configuration.

In the equations above, the system is assumed to be time-invariant. The algorithm can, however, be readily extended to time-variant systems by replacing the system matrices **A**, **B**, **G**, and **J**, with the system matrices $\mathbf{A}_{[k]}$, $\mathbf{B}_{[k]}$, $\mathbf{G}_{[k]}$, and $\mathbf{J}_{[k]}$, that depend on the time step k.

3 MEASUREMENT SETUP

The structure under consideration in this paper is a footbridge, located in Ninove (Belgium). The two-span cable-stayed steel bridge, shown in figure 1, has a main and secondary span of 36 m and 22.5 m, respectively.

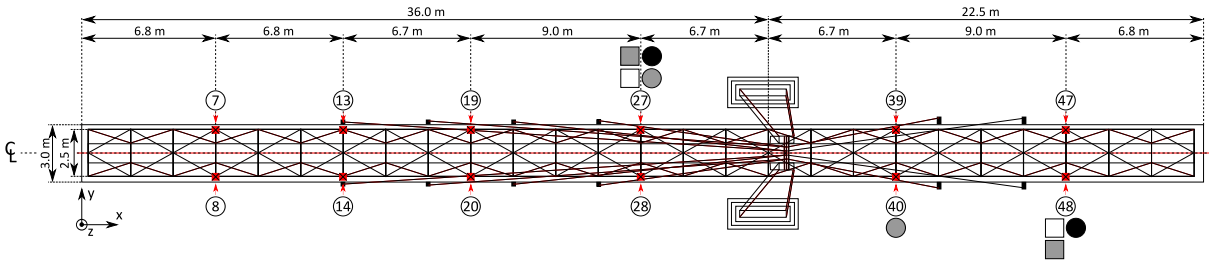

Figure 2: Sensor configuration (white circle: GMS-18 unit, black circle: uniaxial accelerometer, gray circle: optical displacement sensor, white square: instrumented hammer, gray square: load cell).

Figure 1: The footbridge in Ninove, Belgium.

Three different types of excitation have been considered in the experiments: (1) ambient excitation, mainly consisting of wind loads, (2) excitation by hammer impacts, and (3) excitation by pneumatic actuators developed by the Acoustics and Vibration Research Group of the Vrije Universiteit Brussel (Deckers et al. 2008). Figure 2 shows the sensor configuration. The acceleration response of the footbridge has been recorded in three orthogonal directions at 12 locations on the bridge deck, using 12 wireless GeoSIG GMS-18 units. In addition, a National Instruments (NI) data acquisition system has been used to record (1) the vertical acceleration at nodes 27 and 48, obtained from PCB 393B04 uniaxial accelerometers, (2) the vertical displacement of the bridge deck at nodes 27 and 40, obtained from AWLG 008M optical displacement sensors, (3) the impact loads applied vertically at nodes 27 and 48 using PCB 086D50 instrumented hammers (mass 5.5 kg), and (4) the tension forces applied vertically by the pneumatic actuators using a PCB 222B load cell and a BD 5 load cell.

A sampling frequency of 200 Hz and 1000 Hz is used for the GMS-18 units and the NI system, respectively. The GMS-18 acceleration data and the measurement data obtained from the NI system are synchronized by maximizing the correlation between the acceleration obtained from the GMS-18 unit at node 48 and the acceleration at node 48 obtained from the cabled uniaxial accelerometer. The measured response and force signals used in the analysis are all digitally lowpass filtered by means of an eighth-order Chebyshev type I lowpass filter with a cut-off frequency of 16 Hz, in both the forward and the reverse direction to remove all phase distortion, and then resampled at 40 Hz. Next, the acceleration signals obtained from the NI system and the GMS-18 units are additionally digitally highpass filtered by means of a fifth order Butterworth filter with a cut-off frequency of 0.5 Hz and 0.1 Hz, respectively, in both the forward and the reverse direction. The aim of the filter is to remove the low frequency components from the signals that are contaminated by measurement noise. Finally, a detrend operation is applied to all acceleration signals to remove the (physically meaningless) DC component. The measured displacement signals are relative to the displacement at the start of the experiment.

4 SYSTEM MODEL

The force identification is based on a state-space description of the system, given by equations (1) and (2). The system model used in the present analysis is based on a detailed finite element (FE) model of the structure, that is built using the FE program ANSYS. The FE model is calibrated using a set of experimental modal parameters that have been obtained through operational modal analysis (OMA) (Peeters & De Roeck 1999, Reynders & De Roeck 2008). In total 18 modes of the bridge deck have been identified in the frequency range from 0 Hz to 20 Hz. Table 1 gives the natural frequencies, the modal damping ratios, and a description of the mode shapes corresponding to the identified modes. Comparison of the experimental modal parameters with the modal parameters obtained from the initial FE model shows some discrepancies. A model calibration is therefore performed. The calibration parameters considered in this analysis are (1) the stiffnesses of the neoprene bearings, (2) the Young's modulus of the bridge deck, (3) the Young's modulus of the pylons, and (4) the effective Young's modulus of the cables. The natural frequencies and mode shapes corresponding to 14 identified modes are used as the observed quantities in the calibration procedure, i.e. modes 1 – 5, 7 – 9, 11 – 13, and 15 – 17, listed in table 1. The remaining modes, i.e. modes 6, 10, 14, and 18, are used for cross validation of the model after calibration.

Figure 3 shows modes 1, 3, and 7 obtained from the calibrated FE model. Table 1 shows the modal characteristics obtained from the FE model after calibration and a comparison to the corresponding observed quantities. The relative error on the natural frequency ε_j for mode j is defined as $\varepsilon_j = (f_j - \tilde{f}_j)/\tilde{f}_j$, where f_j is the undamped natural frequency corresponding

to mode j, obtained from the FE model, and $\tilde{f}_j$ is the corresponding value obtained from the system identification. In general very high MAC-values (MAC ≥ 0.89) are obtained, both for the modes included in the model calibration and the modes used for cross validation. This indicates a good overall agreement between the identified dynamic behavior of the footbridge and the one predicted by model.

A reduced-order discrete-time state-space model is constructed from the modal characteristics of the structure. The model includes all bending modes of the bridge deck with a natural frequency that falls within the frequency range 0 Hz to 20 Hz, i.e. the 18 modes listed in table 1. For each mode, the mass normalized mode shape of the FE model is used. The natural frequency and modal damping ratio are taken as the experimentally identified values. A zero order hold assumption is applied on the input vector $\mathbf{p}_{[k]}$ in the time discretization. The reader is referred to (Maes et al. 2016) for the expression of the system matrices **A**, **B**, **G**, and **J**.

5 SELECTION OF DATA FOR FORCE IDENTIFICATION

The sensor configuration for force identification is to be determined such that (1) the conditions for instantaneous system inversion (Maes et al. 2015) are met, and (2) the uncertainty on the force estimates introduced by measurement noise and wind loads is (sufficiently) small.

5.1 *Invertibility conditions*

The invertibility of a linear system model in general depends on three conditions. Firstly, the dynamic forces and/or corresponding states must be identifiable from the data. Secondly, the system inversion algorithm must be stable, such that small perturbations in the data do not give rise to unbounded errors on the identified forces and the system states. Thirdly, the estimates must be uniquely defined by the data. The general conditions for system inversion were recently translated into a number of requirements on the sensor network, i.e., sensor types, sensor locations, and number of sensors, for the specific case of linear modally reduced order models (Maes et al. 2015). The invertibility conditions, derived assuming no noise, are necessary but not sufficient for guaranteeing that the forces and system states can be identified in the presence of noise.

In this study, the aim is to estimate vertical forces at nodes 27 and 48 (see figure 2), denoted by p27z and p48z. A selection of data is made from the complete data set, including all response measurements on the bridge deck as listed in section 3. The displacements are denoted by d27z and d40z, the accelerations obtained from the NI system by a27ni and a48ni. The accelerations obtained from the GMS-18 units are denoted by a$j\zeta$, where j refers to the node number in the measurement grid, and ζ denotes the measurement direction (y or z).

Using the techniques proposed in (Maes et al. 2015), a minimum subset of output data is determined, which allows for the estimation of the forces. In this case, at least two (n_p) accelerations and two (n_p) displacements are required to ensure a coupling between the estimated forces and the measured acceleration and displacement data, respectively, through two (n_p) modes. The two displacements, d27z and d40z, have to be included in the data vector in order to obtain a stable system inverse with a unique solution. Additional accelerations are required for instantaneous system inversion. In the following, the data used for joint input-state estimation consists of two collocated acceleration measurements a27ni and a48ni and two displacement measurements d27z and d40z. For this data set, all invertibility conditions are met, and these will still hold when more measurements are added. The reader is referred to (Maes et al. 2015) for detailed information on the design of the sensor network.

5.2 *Quantification of uncertainty*

The uncertainty on the force estimates obtained from joint input-state estimation, introduced by wind excitation and measurement noise, is assessed by means of the uncertainty quantification approach introduced in (Maes et al. 2016). Quantification of the uncertainty requires the power spectral density (PSD) of the unknown stochastic excitation, that has been obtained from the response of the structure under ambient loading. The noise covariance matrices **Q**, **R**, and **S** used for joint input-state estimation are based on the PSD of the unknown stochastic excitation and the noise characteristics of the sensors.

Table 2 compares the estimated force error variance for two data sets: set 1 is the minimum set including two collocated accelerations and two displacements (4 sensors) that was introduced in section 5.1; set 2 includes all response measurements on the bridge deck (40 sensors). The error variance is obtained considering the estimation errors in the frequency range from 0.2 to 16 Hz. The error variance for data set 2 is only slightly lower than the error variance for the minimum data set 1. In this case, using an extensive data set only produces minor benefits.

6 RESULTS FORCE IDENTIFICATION

This section presents the results of the joint input-state estimation for the identification of impact, harmonic, and swept sine excitation applied to the bridge deck. The forces are estimated using the minimum data set consisting of two displacements and two accelerations introduced in section 5. The noise covari-

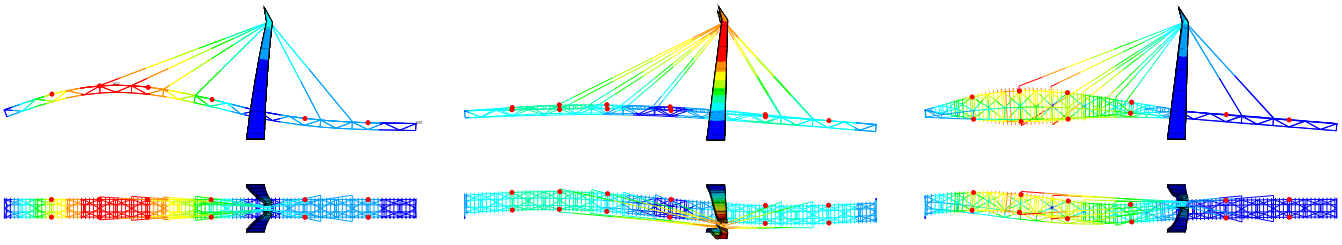

Figure 3: Mode shape mode 1 (left), mode 3 (middle), and mode 7 (right) obtained from the calibrated FE model (top: side view, bottom: top view). The measurement locations are indicated by red dots.

j	$\tilde{f}_j$ [Hz]	$\tilde{\xi}_j$ [%]	j_{fem}	f_j [Hz]	ε_j [%]	MAC [-]	Description
1	2.93	1.16	2	3.07	4.70	1.00	1st lateral bending main span
2	2.97	0.39	1	2.87	-3.64	1.00	1st vertical bending main span
3	3.81	0.77	3	3.73	-2.11	0.99	1st combined lateral bending
4	5.79	1.04	4	5.50	-4.98	0.89	1st lateral bending secondary span
5	6.00	0.52	5	5.81	-3.09	0.98	1st vertical bending secondary span
6†	7.06	0.20	7	7.07	0.08	0.94	1st torsional main span
7	7.27	1.26	6	6.84	-5.95	0.96	2nd lateral bending main span
8	8.02	0.56	8	7.62	-5.00	0.99	2nd vertical bending main span
9	9.83	0.73	11	9.97	1.38	0.94	2nd combined lateral bending
10†	11.06	1.28	12	10.80	-2.39	0.96	1st torsional secondary span
11	11.44	2.09	13	11.60	1.38	0.94	2nd torsional main span
12	12.57	1.40	14	12.92	2.72	0.97	3rd combined lateral bending
13	13.59	0.41	15	13.07	-3.85	0.98	3rd vertical bending main span
14†	14.08	0.47	16	14.07	-0.12	0.93	3rd lateral bending main span
15	14.72	0.34	17	14.18	-3.68	0.98	2nd vertical bending secondary span
16	16.20	0.94	19	16.84	3.98	0.97	4th lateral bending main span
17	17.55	1.33	21	18.71	6.61	0.90	2nd torsional secondary span
18†	18.63	0.68	20	17.86	-4.17	0.93	4th vertical bending main span

Table 1: Comparison between the experimentally identified modal characteristics and the modal characteristics calculated from the calibrated FE model (j: No. identified mode, $\tilde{f}_j$: identified undamped natural frequency, $\tilde{\xi}_j$: identified modal damping ratio, j_{fem}: No. corresponding mode calibrated FE model, f_j: undamped natural frequency FE model, ε_j: relative error f_j w.r.t. $\tilde{f}_j$, MAC: MAC-value). The identified modes indicated with a dagger are not included in the calibration, but used for cross validation.

Table 2: Estimate of the steady-state force error variance (frequency range 0.2 to 16 Hz) for two different sets of sensors. $\tilde{p}_{i[k|k]}$ represents the error on the time history of the vertical force at node i.

	set 1	set 2
Sensors	d27z, d40z, a27ni, a48ni	d27z, d40z, a27ni, a48ni, a$j\zeta$
Var($\tilde{p}_{27[k\|k]}$) [N^2]	4.39	2.89
Var($\tilde{p}_{48[k\|k]}$) [N^2]	6.86	6.58
Total variance [N^2]	11.25	9.47

ance matrices $\mathbf{Q}$, $\mathbf{R}$, and $\mathbf{S}$ used in the force identification are identical to those computed in section 5.2. The initial state estimate vector $\mathbf{x}_{[0|-1]}$ and its error covariance matrix $\mathbf{P}_{[0|-1]}$ are both assumed zero.

Figure 4 shows the results of the identification for a sequence of hammer impacts applied at nodes 27 and 48. A fairly good estimate of both forces is seen from both the time history and the frequency content. Three time intervals can be distinguished in figures 4b and 4e for a single hammer impact applied to the bridge deck; (1) the impact, (2) free vibration, and (3) ambient vibration. During the impact, the broadband hammer force excites the entire frequency range considered. The errors introduced by ambient forces (i.e. unknown stochastic forces) are small, since the hammer impact is far more important than the ambient loading. During the free vibration phase, the structure vibrates at its natural frequencies and modeling errors manifest in errors on the estimated force time history that generally decay exponentially over time. It is seen from figures 4a and 4d that this free vibration phase, characterized by force amplitudes that clearly decay exponentially over time, takes 30 to 40 seconds, depending on the amplitude of the hammer impact applied. After the free vibration phase, the measured response is predominantly due to ambient loads. The ambient vibration phase is, for example, seen in figures 4b and 4e for $t < 104$ s. During this phase, the uncertainty on the estimated forces stems from ambient excitation and measurement errors. As expected, the force levels observed during this phase (i.e. the force error levels) are small and in line with the estimated error statistics obtained from the uncertainty quantification approach in section 5.2 (see table 2: $\sigma_{\tilde{p}_{27}} = \sqrt{4.39\ \text{N}^2} = 2.10\ \text{N}$, $\sigma_{\tilde{p}_{48}} = \sqrt{6.86\ \text{N}^2} = 2.62\ \text{N}$). It is concluded that the errors introduced by the ambient excitation and the measurement errors are small compared to the peak values generated by the impact forces. From the time history of the forces in figures 4b and 4e, it is also seen that, in this case of broadband excitation, the al-

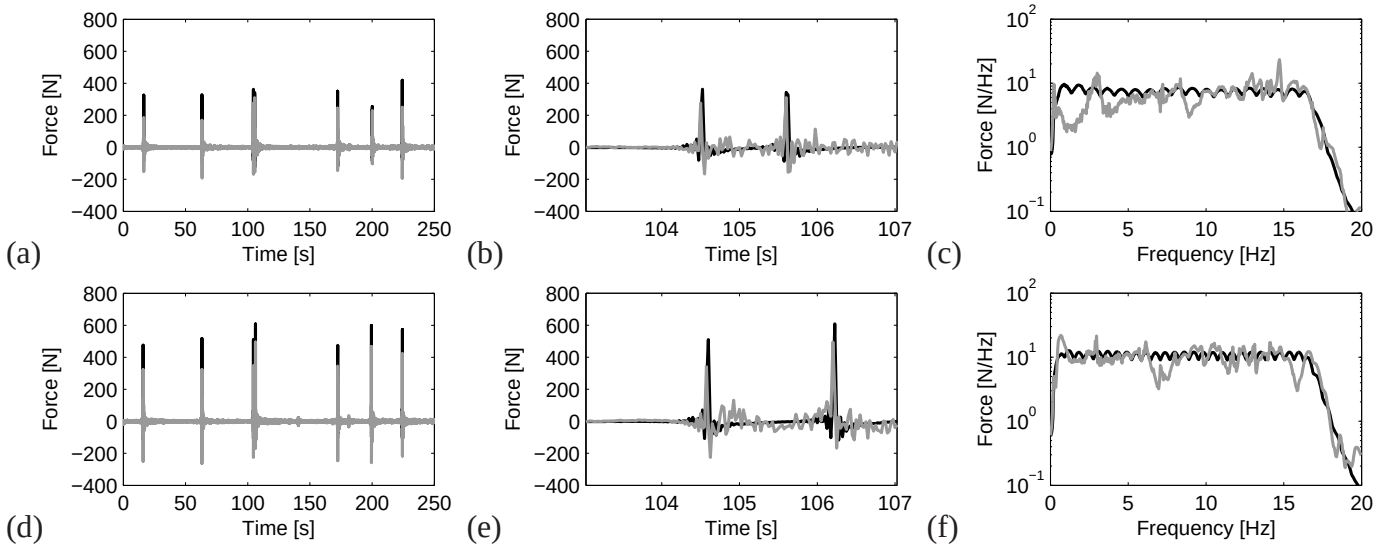

Figure 4: Time history (left), detail of the time history (middle), and averaged amplitude of the narrow band frequency spectrum (right) of the impact forces applied at node 27 ((a) – (c)) and node 48 ((d) – (f)), sensor set 1. The measured force signals are shown in black, the identified force signals are shown in gray.

gorithm is able to properly distinguish between the two forces.

Figure 5 shows the results for the identification procedure for two harmonic forces, applied at nodes 27 and 48. The dominant excitation frequency of the force applied at node 27 is 8 Hz, whereas the dominant excitation frequency of the force applied at node 48 is 6 Hz. In this case where the excitation is dominated by a limited number of frequencies, modeling errors occurring at the excitation frequencies prohibit a proper distinction between the two independent forces. The identified force at node 48 clearly contains an important harmonic component at 8 Hz, which is less pronounced in the measured force signal.

Figure 6 shows the results of the identification procedure for two swept sine forces, applied at nodes 27 and 48. The excitation frequency of the force applied at node 27 rises from 0.5 Hz to 10 Hz in 285 s, whereas for node 48, the excitation frequency rises from 0.375 Hz to 7.5 Hz in the same time period. The excitation frequency of the forces applied at nodes 27 and 48 is increased in steps of 1 mHz and 0.75 mHz every 30 ms, respectively. Two cycles of 285 s are considered. The response of the structure depends on the rate at which the frequency increases, i.e. 1/30 Hz/s for the force applied at node 27 and 1/40 Hz/s for the force applied at node 48. For each frequency step, the response of the structure evolves from harmonic vibration at the previous excitation frequencies to harmonic vibration at the current excitation frequencies. When the excitation frequency is slowly increased, the response achieves steady-state before the excitation frequency is changed again, whereas if the excitation frequency is rapidly increased, the response is mainly dominated by transient phenomena. In the transition phase, the structure primarily vibrates at its natural frequencies and the errors are comparable to those observed in the free vibration phase following impact excitation. In addition, modeling errors at the excitation frequency result in errors on the estimated stationary forces. As in the case of harmonic excitation, modeling errors prohibit a proper distinction between the two forces, resulting in large errors on the estimated forces for some frequencies.

7 CONCLUSIONS

This paper presents a verification of a joint input-state estimation algorithm, using data obtained from in situ experiments on a footbridge. The joint input-state estimation algorithm is used for the identification of impact, harmonic, and swept sine forces applied to the bridge deck. A dynamic model of the structure has been composed using a detailed finite element model of the structure, which was calibrated using a set of experimental modal characteristics. The uncertainty introduced by wind loads and measurement noise is quantified based on the power spectral density of the ambient forces, which is identified from the response of the structure under ambient loading. Verification of the results is carried out by comparing the estimated forces with the actual measured forces. For the case of broadband impact loading, the forces obtained from joint input-state estimation are in good agreement with the true, measured forces. Although good overall agreement is also observed between the estimated and measured forces for harmonic and swept sine loads, modeling errors in this case are found to prohibit a proper distinction between the multiple independent forces.

ACKNOWLEDGMENTS

The research presented in this paper has been performed within the framework of the project

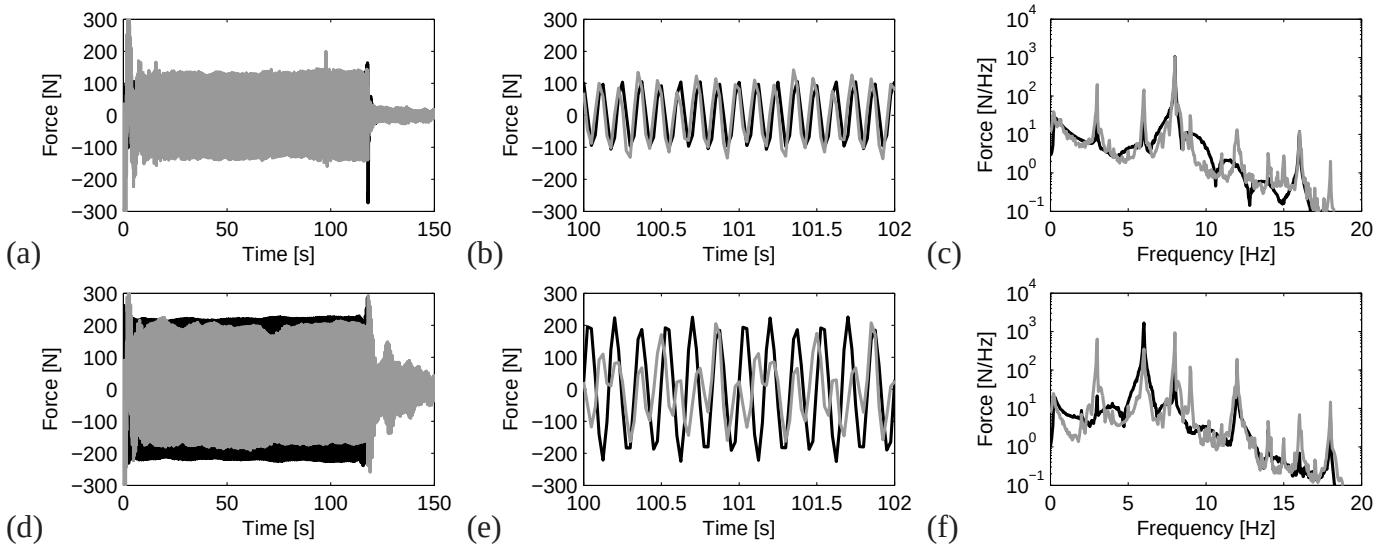

Figure 5: Time history (left), detail of the time history (middle), and averaged amplitude of the narrow band frequency spectrum (right) of the harmonic forces applied at node 27 ((a) – (c)) and node 48 ((d) – (f)), sensor set 1. The measured force signals are shown in black, the identified force signals are shown in gray.

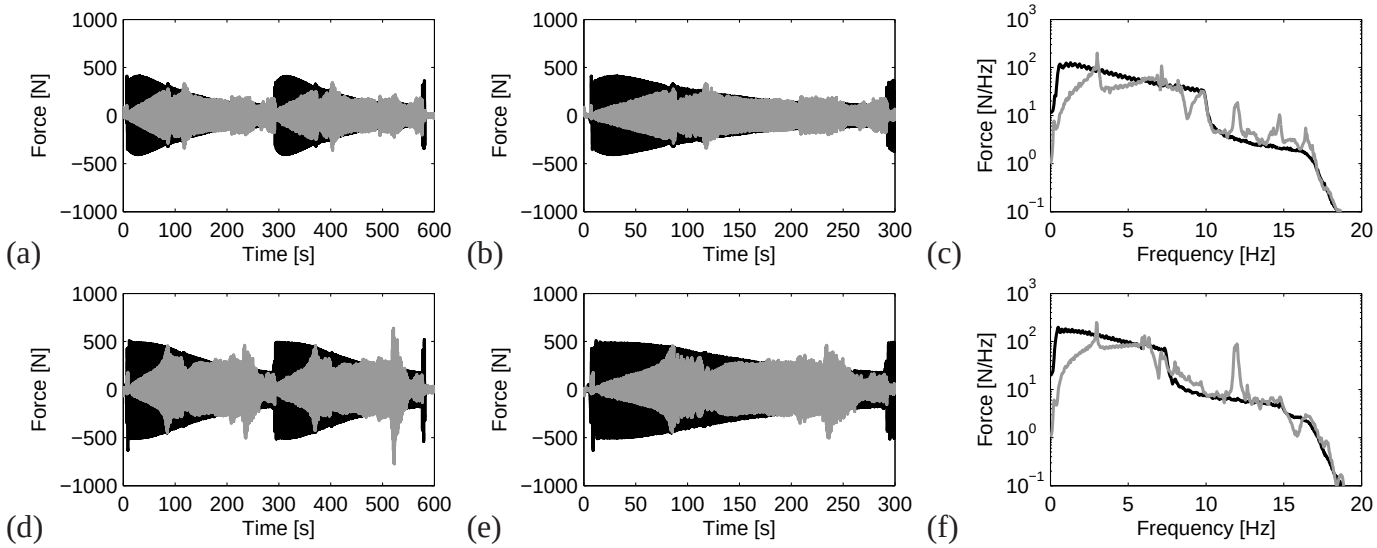

Figure 6: Time history (left), detail of the time history (middle), and averaged amplitude of the narrow band frequency spectrum (right) of the swept sine forces applied at node 27 ((a) – (c)) and node 48 ((d) – (f)), sensor set 1. The measured force signals are shown in black, the identified force signals are shown in gray.

G.0738.11 “Inverse identification of wind loads on structures”, funded by the Research Foundation Flanders (FWO), Belgium. Their financial support is gratefully acknowledged. The authors affiliated to KU Leuven are all members of the KU Leuven - BOF PFV/10/002 OPTEC - Optimization in Engineering Center.

REFERENCES

Bernal, D. & A. Ussia (2015). Sequential deconvolution input reconstruction. *Mechanical Systems and Signal Processing 50–51*, 41–55.

Ching, J. & J. Beck (2007). Real-time reliability estimation for serviceability limit states in structures with uncertain dynamic excitation and incomplete output data. *Probabilistic Engineering Mechanics 22*, 50–62.

Deckers, K., P. Guillaume, D. Lefeber, G. De Roeck, & E. Reynders (2008, February). Modal testing of bridges using low-weight pneumatic artificial muscle actuators. In *Proceedings of IMAC 26, the International Modal Analysis Conference*, Orlando, FL.

Eftekhar Azam, S., C. Papadimitriou, & E. Chatzi (2015). A dual Kalman filter approach for state estimation via output-only acceleration measurements. *Mechanical Systems and Signal Processing 60–61*, 866–886.

Gillijns, S. & B. De Moor (2007). Unbiased minimum-variance input and state estimation for linear discrete-time systems with direct feedthrough. *Automatica 43*(5), 934–937.

Hernandez, E. (2011). A natural observer for optimal state estimation in second order linear structural systems. *Mechanical Systems and Signal Processing 25*(8), 2938–2947.

Hernandez, E. & D. Bernal (2008). State estimation in structural systems with model uncertainties. *ASCE Journal of Engineering Mechanics 134*(3), 252–257.

Hsieh, C.-S. (2010). On the global optimality of unbiased minimum-variance state estimation for systems with unknown inputs. *Automatica 46*, 708–715.

Klinkov, M. & C. Fritzen (2007). An updated comparison of the force reconstruction methods. *Key Engineering Materials 347*, 461–466.

Klinkov, M. & C.-P. Fritzen (2006, September). Online estimation of external loads from dynamic measurements. In P. Sas and M. D. Munck (Eds.), *Proceedings ISMA2006*, Leuven,

Belgium, pp. 3957–3968.

Liu, Y. & W. Shepard (2005). Dynamic force identification based on enhanced least squares and total least squares schemes in the frequency domain. *Journal of Sound and Vibration 282*, 37–60.

Lourens, E., C. Papadimitriou, S. Gillijns, E. Reynders, G. De Roeck, & G. Lombaert (2012). Joint input-response estimation for structural systems based on reduced-order models and vibration data from a limited number of sensors. *Mechanical Systems and Signal Processing 29*, 310–327.

Lourens, E., E. Reynders, G. De Roeck, G. Degrande, & G. Lombaert (2012). An augmented Kalman filter for force identification in structural dynamics. *Mechanical Systems and Signal Processing 27*, 446–460.

Maes, K., E. Lourens, K. Van Nimmen, E. Reynders, G. De Roeck, & G. Lombaert (2015). Design of sensor networks for instantaneous inversion of modally reduced order models in structural dynamics. *Mechanical Systems and Signal Processing 52–53*, 628–644.

Maes, K., A. Smyth, G. De Roeck, & G. Lombaert (2016). Joint input-state estimation in structural dynamics. *Mechanical Systems and Signal Processing 70–71*, 445–466.

Nordström, L. & T. Nordberg (2002). A critical comparison of time domain load identification methods. In *Proceedings of the 6th International Conference on Motion and Vibration Control*, Saitama, Japan, pp. 1151–1156.

Papadimitriou, C., C.-P. Fritzen, P. Kraemer, & E. Ntotsios (2011). Fatigue predictions in entire body of metallic structures from a limited number of vibration sensors using Kalman filtering. *Structural Control and Health Monitoring 18*, 554–573. Published online in Wiley InterScience (www.interscience.wiley.com).

Parloo, E., P. Guillaume, & M. Van Overmeire (2003). Damage assessment using mode shape sensitivities. *Mechanical Systems and Signal Processing 17*(3), 499–518.

Peeters, B. & G. De Roeck (1999). Reference-based stochastic subspace identification for output-only modal analysis. *Mechanical Systems and Signal Processing 13*(6), 855–878.

Reynders, E. & G. De Roeck (2008). Reference-based combined deterministic-stochastic subspace identification for experimental and operational modal analysis. *Mechanical Systems and Signal Processing 22*(3), 617–637.